University of Glasgow

Guerrero-Martinez, F. J., Karimi, N. and Ramos, E. (2018) Numerical modeling of multiple steady-state convective modes in a tilted porous medium heated from below. *International Journal of Heat and Mass Transfer*, 92, pp. 64-72. (doi:10.1016/j.icheatmasstransfer.2018.02.009)

This is the author's final accepted version.

There may be differences between this version and the published version. You are advised to consult the publisher's version if you wish to cite from it.

http://eprints.gla.ac.uk/156841/

Deposited on: 06 February 2018

Enlighten – Research publications by members of the University of Glasgow
http://eprints.gla.ac.uk

Numerical modeling of multiple steady-state convective modes in a tilted porous medium heated from below

Fernando J. Guerrero-Martínez[a,1], Nader Karimi[a,b,*], Eduardo Ramos[c]

[a] *School of Engineering, University of Glasgow, Glasgow G12 8QQ, Scotland, UK.*
[b] *School of Computing and Engineering, Civil and Mechanical Engineering Department, University of Missouri-Kansas City, Kansas City, MO, 64110, USA*
[c] *Renewable Energy Institute, Universidad Nacional Autónoma de México, 62580 Temixco, Mor. Mexico*

Abstract

Numerical simulations are carried out to determine the steady-state convective modes in a rectangular porous cavity heated from below. The property of multiplicity of solutions for a given set of governing parameters is examined in this paper. The multiple steady-state solutions that appear in a horizontal cavity for a given Rayleigh number are obtained by means of suitable initial conditions. Each of these solutions is then perturbed by increasing the inclination angle in order to identify the transition angle to a different convective mode. It is observed that for an odd-number of convective cells, if the counterclockwise rotating cells dominate the configuration, the Nusselt number increases with the slope angle up to a maximum and then decreases before the transition to single cell convection. Otherwise, if there are more clockwise rotating cells, the Nusselt number decreases monotonically and the configuration becomes unstable. Since multicellular configurations with even number of convective cells have equal number of clockwise and counterclockwise rotating cells, this case presents a single behavior characterized by a decrease in the Nusselt number. The transition angles from multicellular to single cell convection are found to be as large as 45° when the aspect ratio of the cavity is large, so that this angle

---

*Corresponding author. Tel.: +1 816 235 1499
Email address: nader.karimi@glasgow.ac.uk (Nader Karimi)
[1] Present address: Geophysics Institute, Universidad Nacional Autónoma de México, Cd. Universitaria, México D.F., 04510, México

Preprint submitted to International Communications in Heat and Mass Transfer February 5, 2018

is the upper limit to destabilize multicellular convection.

Keywords: 2D numerical modeling, porous medium, free convection, Boussinesq approximation.

Nomenclature

Greek symbols

α	Slope angle
β	Thermal expansion coefficient
η	Overall thermal diffusivity
μ	Viscosity
ψ	Stream function
ρ	Density
σ	Ratio of solid-fluid heat capacities
θ	Dimensionless temperature

Other symbols

$-$	Overbar denotes dimensional variable

Roman letters

$\mathbf{u}$	Darcy's velocity
$\hat{A}$	Amplitud
B	Characteristic length
C	Length
D	Aspect ratio
g	Gravitational constant

k Permeability

L_∞ Infinity norm

n Number of convective cells

Nu Nusselt number

P Pressure

Ra Darcy-Rayleigh number

T Temperature

t Time

x, y, z Cartesian coordinates

Subscripts

0 Reference quantity

c Critical quantity

int Simulation time interval

l Local

ss Steady state

t Transition

1. Introduction

Extensive research on free convection in porous media has been carried out in the past due to its importance in different scientific and engineering contexts. For instance, modelign of low enthalpy geothermal systems is a research area closely related with this topic [1, 2, 3]. In last years this problem has been addressed from a variety of perspectives. Baytaş and Pop [4] studied free convection in oblique porous enclosures. Baytaş [5] and Meshram [6] considered entropy generation effects in an inclined porous cavity. Khanafer [7] looked into non-Darcian effects in free convection in a porous medium. Bennacer et al. [8] conducted anisotropy studies in a vertical porous enclosure with double diffusive convection. Free convection in porous media in conditions of turbulent flow and mass transport has also been studied [9, 10]. De Lemos [11] incorporated non-thermal equilibrium conditions, and more recently Carvalho and de Lemos analyzed the case of free convection in laminar flow and mass transport assuming also non-thermal equilibrium conditions [12]. Although these works explore different aspects of the physics that govern free convection in porous media, some questions regarding the steady state convective modes that arise in 2D in such systems are still unanswered. For instance, whereas multicellular and single cell convective modes are well known, the different forms multicellular convection can adopt has not been reported in detail. The transition angles of these convective modes to single cell have not been reported either. The numerical study presented here determines the multiple steady-state convective modes that exist in such a system and their transition angles. At the same time this work aims to provide a wider perspective for the analysis of steady-sate free convection in porous media in three-dimensions (3D) [13, 14].

Fundamental aspects of the problem analyzed here are given by the solution of the Horton-Rogers-Lapwood problem [15]. This problem establishes the conditions for the onset of convection in a horizontal porous layer heated from below. The early works by Horton and Rogers [16] and Lapwood [17] determined a critical Rayleigh number ($Ra_c = 4\pi^2$) for the onset of convection in such a system. Elder [18] presented one of the first numerical and experimental studies of steady-state convection for this problem. He described the steady state cellular motion of the fluid, incorporating edge-effects of the porous enclosure. Straus [19] conducted stability analysis and reported that as the Rayleigh number increases the wavenumber of the system increases, and for $Ra \geq 380$ there are no stable 2D solutions. Likewise, De La Torre Juárez and Busse [20] showed that the maximum Nusselt number of steady state convection corresponds to higher wavenumbers as Ra increases.

Kaneko et al. [21] carried out an experimental study of free convection in an inclined porous enclosure. They found that there is an angle at which the system reaches the maximum level of convective motion, characterized by multiple convective cells. They also reported that above this angle the system evolves towards single cell convection. This transition between multicellular and single cell convection was addressed numerically by Moya et al. [22]. They analyzed the change of the sateady state solutions as the slope angle and Rayleigh number were varied. Their model successfully reproduced the appearance of single-cell convection as it was shown experimentally by Bories and Combarnous [23], however due to the steady-state numerical scheme they were only able to obtain a limited number of multicellular conective modes. This arises the question that what are the possible multicellular configurations before reaching single-cell convection. The existence of multiplicity of steady state solutions was described by Sen et al. [24], who reported that multiple steady states exist when the inclinations with respect to the heated wall are small enough and some of which are unstable. Riley and Winters [25] described the mechanisms through which the multiple solutions reduce to leave an apparently unique solution for large slope angles. Rees and Bassom [26] found the maximum inclination angle at which multicellular convection can become unstable, which is $\alpha = 31.49°$ corresponding to a critical Rayleigh number of 104.30. In consistency with this result, Báez and Nicolás [27] calculated transition angles for a Rayleigh number of 100 and different aspect ratios of the porous cavity. Likewise, they observed different multicellular configurations with different number of cells for a given set of governing parameters.

The different multicellular steady state solutions that can exist in a sloping porous enclosure heated from below are found here by inducing the system to host arbitrary numbers of convective cells. This is done by means of providing suitable initial conditions of the governing equations. Each of the induced multicellular configurations will become a steady-state solution as long as such convective mode is stable. Additionally, the evolution of each of these multicellular configurations towards single cell convection is examined by increasing the slope angle in small steps until the solutions destabilize. Unlike previous studies, this work covers a detailed parametric space regarding the slope angle and the number of convective cells in the cavity, which accounts for more than twenty three thousand simulations. The numerical scheme was developed based on the stream function approach, which has been widely applied for the solution of free convection in both porous media and homogeneous fluids [28].

2. Problem formulation

The problem consists of a rectangular porous enclosure of height B and length C with impermeable walls, heated from below, and inclined with an angle α with respect to the horizontal position (Figure 1). The basic assumptions for this problem include local thermal equilibrium, fluid flow is described by Darcy's law, and the Boussinesq approximation is invoked. From these considerations the momentum equation can be stated as follows:

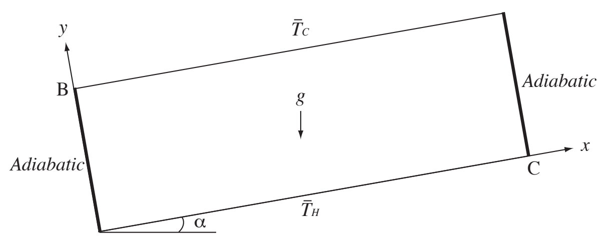

Figure 1: Schematic model of a rectangular porous enclosure tilted an angle α.

$$\bar{\mathbf{u}} = -\frac{k}{\mu}\left(\bar{\nabla}\bar{P} - \rho_0 g \beta_0 (\bar{T} - \bar{T}_0)\mathbf{e}\right) \tag{1}$$

where the vector $\mathbf{e} = (\sin\alpha, \cos\alpha)$ gives account of the components of the buoyancy term in the system. The continuity equation for an incompressible fluid is also recalled

$$\bar{\nabla} \cdot \bar{\mathbf{u}} = 0. \tag{2}$$

Further, the heat transfer equation for the porous medium is written [15]:

$$\sigma\frac{\partial\bar{T}}{\partial\bar{t}}+\bar{\mathbf{u}}\cdot\bar{\nabla}\bar{T}=\bar{\nabla}\cdot(\eta\bar{\nabla}\bar{T}). \tag{3}$$

The problem is nondimensionalized using the following dimensionless variables:

$$x=\frac{\bar{x}}{B},\qquad y=\frac{\bar{y}}{B},\qquad z=\frac{\bar{z}}{B},\qquad P=\frac{k}{\mu\eta}\bar{P},$$

$$\mathbf{u}=\frac{B}{\eta}(\bar{u},\bar{v},\bar{w}),\qquad \theta=\frac{\bar{T}-\bar{T}_0}{\bar{T}_0-\bar{T}_c},\qquad t=\frac{\bar{t}\eta}{\sigma B^2},$$

$$Ra=\frac{Bkg\beta\rho_0}{\eta\mu}(\bar{T}_0-\bar{T}_c),$$

with Ra being the Darcy-Rayleigh number (or simply the Rayleigh number). The dimensionless problem is as follows:

$$\mathbf{u}+\nabla P=Ra\theta\mathbf{e}, \tag{4}$$

$$\frac{\partial\theta}{\partial t}-\nabla^2\theta+\mathbf{u}\cdot\nabla\theta=0, \tag{5}$$

$$\nabla\cdot\mathbf{u}=0. \tag{6}$$

The momentum equation is written in terms of the stream function

$$\Gamma\nabla^2\psi=\left(\frac{\partial\theta}{\partial x}\cos\alpha-\frac{\partial\theta}{\partial y}\sin\alpha\right), \tag{7}$$

where $\Gamma=-1/Ra$.

2.1. Boundary and initial conditions

The boundary conditions for the heat transfer equation read

$$\frac{\partial\theta}{\partial x}=0,\quad \text{for}\quad x=0\quad\text{and}\quad x=D,$$

where D is the aspect ratio C/B, and

$$\theta=1,\quad \text{for}\quad y=0\quad\text{and}\quad t>0,$$

$$\theta = 0, \quad \text{for} \quad y = 1 \quad \text{and} \quad t > 0.$$

Suitable initial conditions can be defined to give rise to a specific number of convective cells n in a horizontal porous enclosure of aspect ratio D. Such initial condition is given by the following function:

$$\theta(x, y) = (1 - y) + \hat{A} \sin(\pi y) \cos\left(\frac{n\pi x}{D}\right), \tag{8}$$

this equation defines a temperature field that is the characteristic of multicellular convection at $\alpha = 0$, with n being the number of cells, and $\hat{A}$ denoting the amplitude of the sinusoidal perturbation. In general the amplitude is defined as $0 < |\hat{A}| < 1$, which is a moderate perturbation of the linear temperature profile $(1 - y)$. In this study, an amplitude $|\hat{A}| = 0.3$ was suitable to give rise to multicellular convection at $\alpha = 0$ for a wide number con convective cells, n, and the three aspect ratios analyzed. Additionally, it is important to note that for a given aspect ratio D and number of cells n, a positive and a negative amplitude give rise to equivalent convective modes as regards n but with opposite direction of rotation of the convective cells.

Regarding the momentum equation, considering that $\psi = 0$ at the boundaries satisfies the condition of impermeable walls, the boundary conditions are

$$\psi = 0, \quad \text{for} \quad x = 0 \quad \text{and} \quad x = D,$$

$$\psi = 0, \quad \text{for} \quad y = 0 \quad \text{and} \quad y = 1.$$

3. Numerical solution

The time-dependent mathematical problem was discretized with the Finite Volume numerical method. The problem requires an iterative solution for each time step for which a fixed point algorithm was implemented. A central differencing scheme was applied for the convective term of the energy equation and a first-order fully implicit scheme was used for the temporal term. A Gauss-Seidel iteration was used for the solution of the algebraic system. The numerical scheme was implemented in Fortran 90 and the simulations were carried out on a PC based on Ubuntu 14.04 with a processor Intel Core i7.

Steady-state solutions were obtained from the evaluation of the convergence of the temperature matrix. The infinity norm of the difference $L_\infty = |\boldsymbol{\theta}^t - \boldsymbol{\theta}^{t-1}|_\infty$ was calculated for successive time steps over a long time interval that proved to be long enough after several tests (2.2×10^4 time steps in this case). The convergence criterion was defined according to the condition $\langle L_\infty \rangle_{t_{int}} < 5 \times 10^{-7}$, where $\langle L_\infty \rangle_{t_{int}}$ is the average infinity norm over the time interval t_{int}.

4. Numerical results and discussion

4.1. Validation

A local Nusselt number (Nu_l) was defined (Eq. 9) to quantify the convective heat transfer throughout the porous enclosure

$$Nu_l = \left| \frac{\partial \theta}{\partial y} \right|_{y=0}, \tag{9}$$

the overall convective heat transfer in the enclosure reads

$$Nu = \int \left| \frac{\partial \theta}{\partial y} \right|_{y=0} dx. \tag{10}$$

A model of aspect ratio $D = 3$ was considered for the validation of the model with a constant Rayleigh number of $Ra = 100$. Three slope angles were analyzed: 10°, 25° and 40°. After a calibration process a time step $\Delta t = 2.0 \times 10^{-4}$ was chosen for the simulations. Additionally, a uniform mesh consisting of $\Delta x = \Delta y = 100^{-1}$ was employed for the spatial discretization. A mesh dependency study showed that a mesh consisting of $\Delta x = \Delta y = 25^{-1}$ leads to equivalent results with a difference of 0.48% in the global Nusselt number.

Table 1 shows a comparison of the model presented here and the results reported by Báez and Nicolás [27]. This table indicates that both the global Nusselt numbers and the convective modes are in agreement. The small difference in the Nusselt number can be attributed to the different mesh size and

Table 1: Nusselt number, Nu, steady-state time, t_{ss}, and number of convective cells, n, of steady-state solutions for the present model and the results reported by Báez and Nicolás [27] for a cavity of aspect ratio $D = 3$.

	Present model			Báez and Nicolás [27]		
α	Nu	t_{ss}	n	Nu	t_{ss}	n
10°	8.36	6.881	3	8.60	0.212	3
25°	6.37	5.226	1	6.75	0.168	1
40°	7.33	4.793	1	7.65	0.338	1

temporal discretization scheme. Additionally, a more rigorous convergence criterion was implemented in the present model in order to ensure that the different convective modes tested in the parametric study are steady state solutions. This criterion gives account of a considerably longer time demanded before establishing the steady state. As mentioned above, the infinity norm is averaged over 2.2×10^4 iterations ($t = 4.4$) which is then compared with the stop condition. Since the convergence criterion is not identical in the compared models, they might not lead to exactly the same result. Nevertheless, the Nusselt numbers show consistency.

4.2. Parametric study

The parameter space considered here consists of three aspect ratios, $D = 3$, 5 and 10, and two Rayleigh numbers, $Ra = 70$ and 100. Slope angles will be considered as follows, the interval $0 \leq \alpha \leq 40°$ will be examined in steps of 0.1°; $40 < \alpha \leq 90°$ in steps of 1° and $90 < \alpha \leq 180°$ in steps of 5°. The initial condition defined in Equation (8) is used only for $\alpha = 0$ for a given number of cells n. The resulting steady-state solution is then used as the initial condition for the next slope angle α and so on.

For $D = 3$, $\alpha = 0$, $Ra = 100$ and $n = 3$ for instance, two initial temperature distributions can be calculated according with either a positive or a negative sign of $\hat{A}$. The corresponding steady-state solutions obtained from these initial conditions are shown in Figure 2. It shows that two steady-state solutions characterized by opposite vorticity signs can be obtained from the same model parameters which is a manifestation of multiplicity of solutions. As a consequence of this property, it is pertinent to analyze the existence of the three-cell multicellular convection for $\alpha > 0$ considering the two forms of the solution.

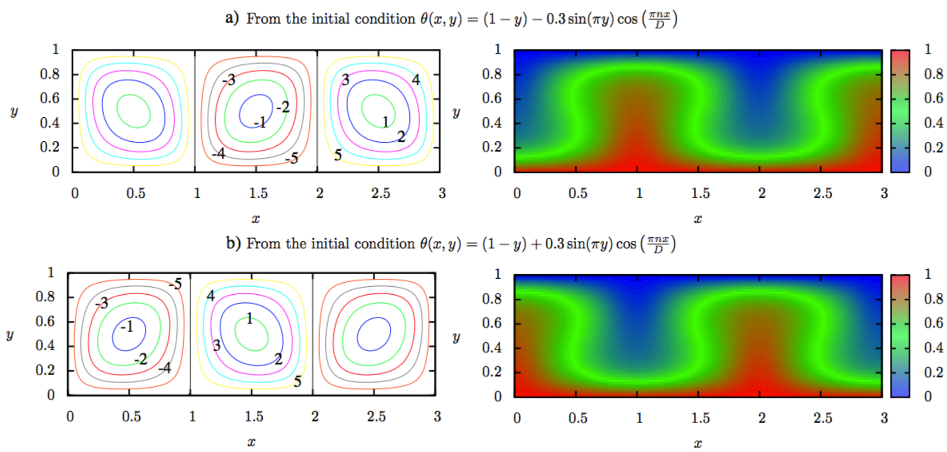

Figure 2: Streamlines and temperature fields of three-cell multicellular convection for $D = 3$, $Ra = 100$ and $\alpha = 0$ obtained from two initial conditions (Eq. 8).

The existence of these three-cell solutions (Figure 2) in the range $\alpha > 0$ was examined here by increasing the angle in steps as described previously. The relation Nu vs α permitted to identify the evolution of the three-cell configurations and the transition to a single cell convective mode. Figure 3 shows this relation for $n = 3$ along with $n = 1$ and $n = 4$. The four-cell solution, $n = 4$, was calculated in the same way as $n = 3$. The one-cell solution however, was obtained from simulations starting at $\alpha = 60°$ with the initial condition given by Equation 8 with $n = 1$, $D = 3$, and $\hat{A}$=-0.3. Then the remaining angles were analyzed moving backwards up to $\alpha = 0$, in this way the minimum angle at which the one-cell solution appears was identified.

Figure 3 shows that the two forms of the three-cell solution evolve in different ways, on the one hand the Nusselt number increases with α for the configuration shown in Figure 2-a ($\hat{A}$=-0.3). The convection in this case consists of two counterclockwise rotating cells. These can be called natural cells, since the fluid next to the hot wall flows upwards, whereas there is one clockwise rotating cell,

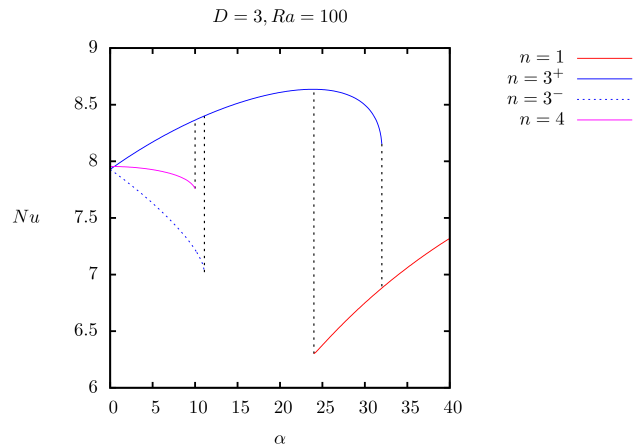

Figure 3: Nu vs α for n = 3, 4, and 1. The solid blue line corresponds to the case $\hat{A}$=-0.3, whereas the dashed blue line in the same interval corresponds to $\hat{A}$=0.3 (Figure 2). The black dashed line shows the transition between number of cells.

or anti-natural cell. This multicellular configuration will be denoted as $n = 3^+$. On the other hand, the configuration shown in Figure 2-b leads to a decrease in the Nusselt number up to 11.1°, where the rotation of the cells is switched to adopt the configuration $n = 3^+$. This decreasing branch of the three-cell solution contains only one natural cell and two anti-natural cells, which explains why the Nusselt number associated with this configuration is low, and why it exists only in relatively small slope angles. Similarly, this configuration will be denoted as $n = 3^-$.

Similar to the three-cell case for $\alpha = 0$, two steady-state solutions were obtained for the four-cell configuration with opposite signs of vorticity, each of the solutions associated with a sign of $\hat{A}$ (Eq. 8). Despite having opposite sign of vorticity, the Nusselt number as a function of α turned out to be the same in both cases: the Nusselt number decreased up to 10° where the convection becomes $n = 3^+$ (Figure 3). This behavior is explained by the fact that both four-cell solutions have two natural and two anti-natural cells, the only difference is their position, so that both cases are equivalent in terms of the heat transfer in the porous enclosure. It can also be observed that there is a zero-slope curve at $\alpha = 0$, unlike the curves for the three-cell configurations.

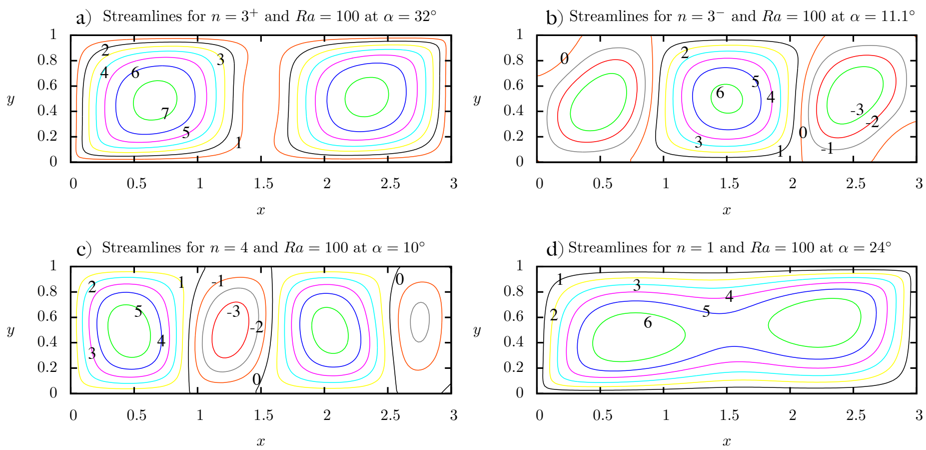

Figure 4: Streamlines of the convective modes $n = 3^+$, $n = 3^-$, $n = 4$, and $n = 1$ at their transition angles to a different configuration.

It is important to observe what happens at the end of the curves, which marks the transition to a different configuration. The Nusselt number for $n = 3^+$ has a maximum at $\alpha = 24°$ and then decreases until the slope tends to infinity. It is expected that the three-cell configuration starts vanishing at this high slope region. Figure 4-a shows the streamlines for this configuration at the transition angle of $\alpha = 32°$, the internal cell has almost disappeared, which resembles a two-cell configuration, yet the two cells have the same direction of rotation characteristic of the three-cell convection. An increase up to $\alpha = 32.1°$ leads to single-cell convection. On the other hand, the transition from $n = 3^-$ to $n = 3^+$ shows a deformation of the external cells at $\alpha = 11.1°$ (Figure 4-b), and then for $\alpha = 11.2°$ the configuration changes to $n = 3^+$. Likewise, for $n = 4$ the external anti-natural cell vanishes (Figure 4-c) and then the configuration changes to $n = 3^+$. Finally, $n = 1$ was observed up to $\alpha = 24°$, which is a single cell with two internal cells (Figure 4-d).

The behavior observed for $n = 3$ and $n = 4$ can be generalized for all the odd and even number of cells at any aspect ratio. Additionally, considering the property of symmetry regarding the rotation of the cavity, the results can be extrapolated to the range $-180° < \alpha < 0$. From these considerations, the cases $n = 1, 2, ..., 5$ were analyzed for $D = 3$, the cases $n = 1, 3, 4, ..., 11$ for $D = 5$, and the cases $n = 1, 7, 8, ..., 19$ for $D = 10$. These convective modes were considered for two Rayleigh numbers $Ra = 70$ and $Ra = 100$.

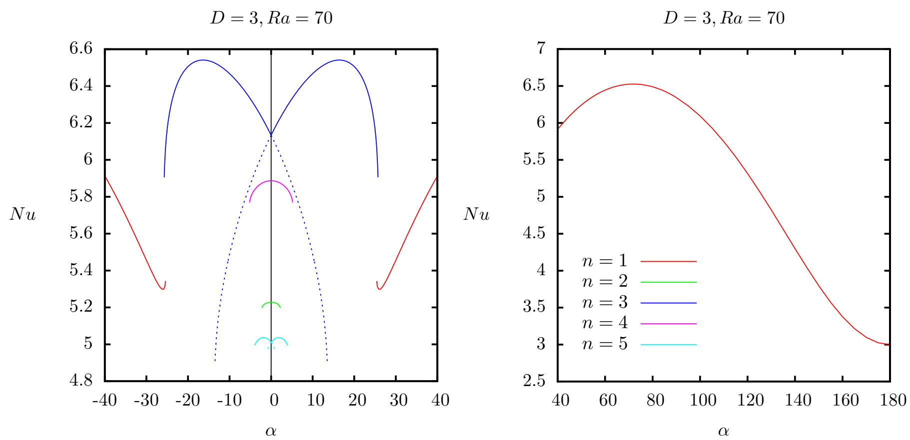

Figure 5: Nusselt number vs slope angle for $n = 1, 2, ..., 5$ convective cells in a 2D porous cavity of aspect ratio $D = 3$ and $Ra = 70$ (for n odd, the dotted line represents the configuration n^- and the continuous line represents n^+).

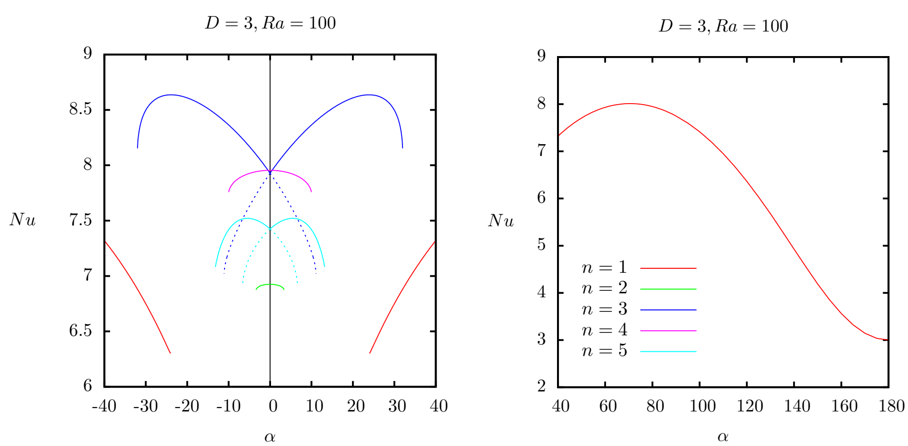

Figure 6: Nusselt number vs slope angle for $n = 1, 2, ..., 5$ convective cells in a 2D porous cavity of aspect ratio $D = 3$ and $Ra = 100$ (for n odd, the dotted line represents the configuration n^- and the continuous line represents n^+).

Figure 5 shows the results for $D = 3$ and $Ra = 70$, it can be observed that the configuration $n = 3^+$ is dominant as regards to the Nusselt number and the range α. The configuration $n = 3^-$ on the other hand, displays a sharp decrease in the Nusselt number, yet it is higher than the one corresponding to $n = 2$, 4, and 5. It can be observed that the one-cell solution presents a bend upwards before the transition, unlike the one-cell curve for $Ra = 100$ (Fig. 3), nevertheless it was confirmed that the convective mode at the end of this curve is once-cell with internal secondary cells, similar in shape to that presented in Figure 4-d. The transition angles for this case are presented in Table 2. Additionally, the curve $n = 1$ displays a sinusoidal-like behavior up to $180°$ reaching a minimum equal to the aspect ratio $D = 3$ at $\alpha = 180°$. Since this case is equivalent to a cavity heated from above there is no convection contributing to the heat transfer throughout the cavity but only conduction, therefore the Nusselt number is equal to the steady-state conductive solution of a cavity with a linear temperature profile $\theta(x, y) = 1 - y$.

Figure 6 shows the results for $Ra = 100$ that was partly described above (Fig. 3). Unlike $Ra = 70$ the maximum Nusselt number at $\alpha = 0$ is associated with an even number of cells, $n = 4$, which is slightly higher than that for $n = 3$. There are, in general, larger transition angles of the convective modes in consistency with a higher Ra, with the exception of $n = 3^-$. The transition angles of the different configurations observed are presented in Table 2. With the exception of $n = 5^-$, which transits to $n = 4$, it can be seen that unstable convective modes switch to $n = 3^+$.

Regarding the transition angles, Rees and Bassom [26] presented a linear stability analysis for the onset of convection in an infinitely long sloping porous layer heated from below. They found the maximum inclination angle at which transverse convective modes can become unstable, to be $\alpha = 31.49032°$ corresponding to a critical Rayleigh number of $Ra_c = 104.30$. This condition is not satisfied by the case $Ra = 100$ for the convective mode $n = 3^+$, which transition occurs at a slightly higher angle of $\alpha = 32°$ (Table 2). This deviation is not unexpected since lateral-boundaries effects are important in this aspect ratio.

Interestingly, even larger transition angles were observed for when higher aspect ratios were considered (Tables 3 and 4), all of them associated with odd number of cells.

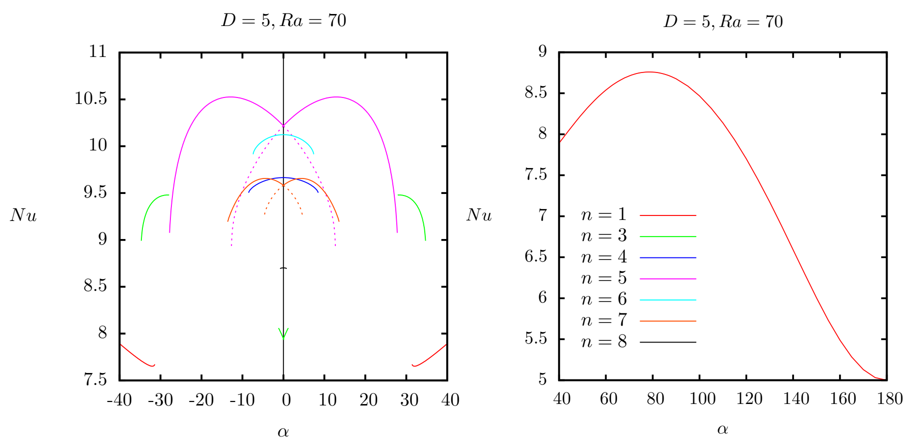

Figure 7: Nusselt number vs slope angle for $n = 1, 3, 4, ..., 8$ convective cells in a 2D porous cavity of aspect ratio $D = 5$ and $Ra = 70$ (for n odd, the dotted line represents the configuration n^- and the continuous line represents n^+).

Figure 7 presents the Nusselt number as a function of α for $D = 5$ and $Ra = 70$ and Figure 8 for $Ra = 100$. For both Rayleigh numbers, the cases $n = 1, 3, 4, ..., 11$ were examined however, for $Ra = 70$, $n = 8$ was the maximum number of cells that comprised a steady-state solution. When comparing Figures

Table 2: Transition angles of the multicellular configurations observed in $D = 3$ for $Ra = 70$ and $Ra = 100$ (the transition to odd number of cells is always to the positive branch n^+).

$D = 3$					
$Ra = 70$			$Ra = 100$		
n	Transition to	α_t	n	Transition to	α_t
1	3	25.4	1	3	24.0
2	3	2.2	2	3	3.4
3^+	1	25.7	3^+	1	32.0
3^-	3	13.5	3^-	3	11.1
4	3	5.2	4	3	10.0
5^+	3	4.0	5^+	3	13.2
5^-	4	0.8	5^-	4	6.6

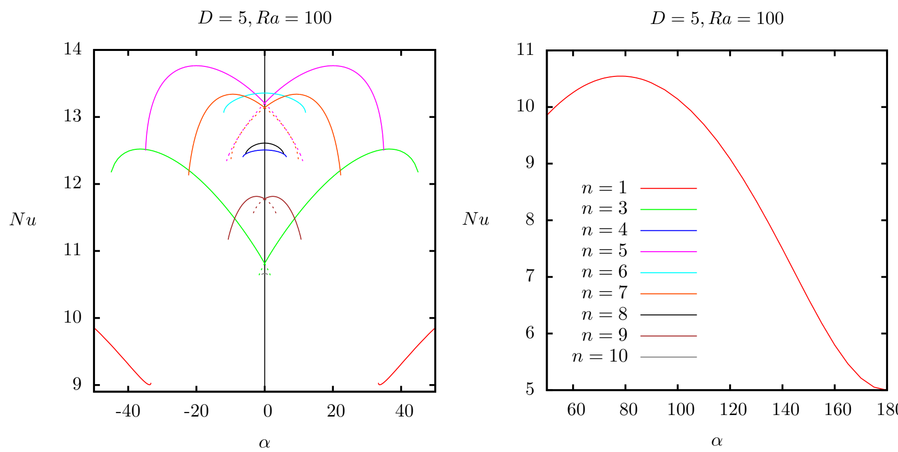

Figure 8: Nusselt number vs slope angle for $n = 1, 3, 4, ..., 11$ convective cells in a 2D porous cavity of aspect ratio $D = 5$ and $Ra = 100$ (for n odd, the dotted line represents the configuration n^- and the continuous line represents n^+).

7 and 8, it can be observed that increasing the Rayleigh number favors the formation of more multicellular configurations, in agreement with Straus [19]. Further, there is in general an increase in the transition angles (Table 3). As regards to $Ra = 70$ (Fig. 7), $n = 5^+$ is a dominant configuration, which terminates at $\alpha = 27.8°$. There is an interesting feature in this graph, $n = 3^+$ is interrupted at $\alpha = 1.2°$ where it becomes $n = 5^+$, and then it appears again at $\alpha = 27.8°$, and finally it changes to $n = 1$ at $\alpha = 34.7°$. Since the Nusselt number for this case is too low at small α, it is possible that in cannot remain as steady state at small inclination angles.

Figures 7 and 8 show that the maximum Nusselt number for $\alpha = 0$ corresponds to $n = 5$ at $Ra = 70$ and $n = 6$ at $Ra = 100$. This increase in the number of cells is consistent with the results reported by De La Torre Juárez and Busse [20] (a similar behavior can be observed for $D = 3$ and $D = 10$). Regarding $Ra = 100$, as α increases $n = 5^+$ becomes the dominant configuration remaining up to $\alpha = 34.9°$ where it becomes three-cell convection (Table 3). It can be observed that as the number of cells increases the corresponding Nusselt number decreases, and so does the range of α for which the particular configuration exists, such is the case of $n = 10$ that appears in a range of inclinations less than $1°$. The highest transition angle observed for $Ra = 100$ is $45°$ corresponding to $n = 3^+$, at this angle the gravitational effects are equally distributed between the x and y axes of the cavity. Finally, both Figure 7 and 8 show a Nusselt number equal to 5 at $\alpha = 180°$. Similar to case $D = 3$, this Nusselt number is equivalent to that obtained from a purely conductive solution $\theta(x, y) = 1 - y$, since the cavity is being heated from the top and cooled from below.

The fact that n-odd multicellular convective modes prevail beyond the critical angle predicted by Rees and Bassom [26] in large aspect ratios is an evidence for the strong convection of these modes. Some forms of multicellular convection can be expected in the range of $31.49° < \alpha < 45°$ since the component of the external force due to gravity is larger on the y-axis than on the x-axis. This favors flow in the y direction so that multiple upwellings and downwellings are formed. An increase of the slope angle beyond $45°$ destabilizes any multicellular convection to give rise to single-cell convection, in response to a larger

Table 3: Transition angles of the multicellular configurations observed in $D = 5$ for $Ra = 70$ and $Ra = 100$ (the transition to odd number of cells is always to the positive branch n^+).

$D = 5$					
$Ra = 70$			$Ra = 100$		
n	Transition to	α_t	n	Transition to	α_t
1	3	31.4	1	3	33.3
3^+	5	1.2	3^+	1	45.0
3^-	4	0.1	3^-	5	1.9
4	5	8.5	4	5	6.4
5^+	3	27.8	5^+	3	34.9
5^-	5	13.1	5^-	7	11.4
6	5	7.4	6	5	12.0
7^+	5	13.6	7^+	5	22.3
7^-	5	4.7	7^-	5	9.9
8	7	0.8	8	7	5.6
—	—	—	9^+	7	10.7
—	—	—	9^-	7	3.6
—	—	—	10	9	0.9

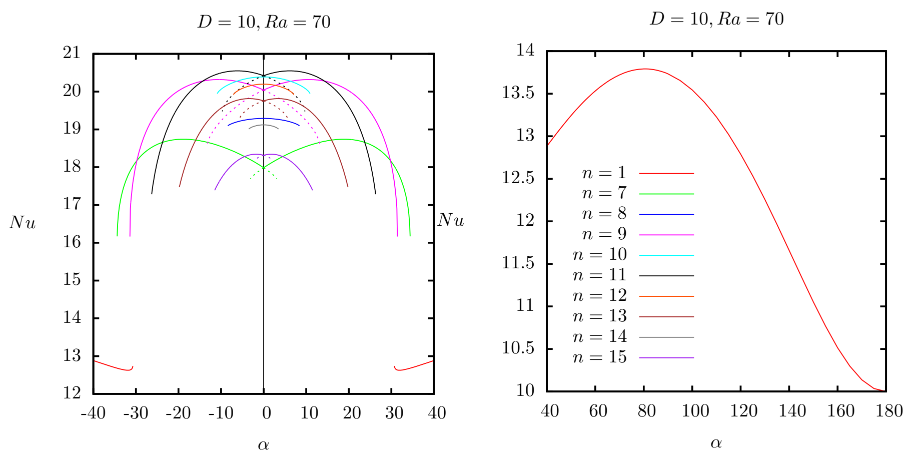

Figure 9: Nusselt number vs slope angle for $n = 1, 7, 8, ..., 15$ convective cells in a 2D porous cavity of aspect ratio $D = 10$ and $Ra = 70$ (for n odd, the dotted line represents the configuration n^- and the continuous line represents n^+).

component of the external force on the x-axis.

The parametric analysis for $D = 10$ is shown in Figures 9 and 10, the cases from $n = 7$ up to $n = 21$ were examined. Between 7 and 15 cells were observed for $Ra = 70$, and between 7 and 21 cells for $Ra = 100$. The cases $n = 20$

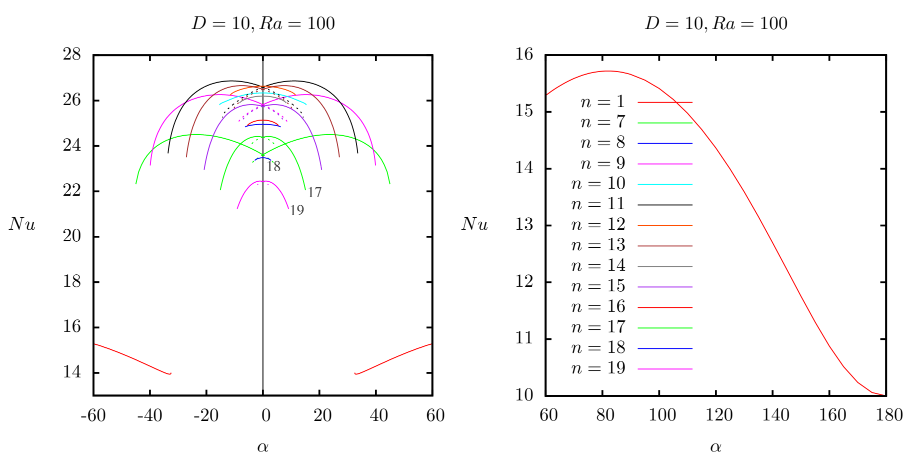

Figure 10: Nusselt number vs slope angle for $n = 1, 7, 8, ..., 19$ convective cells in a 2D porous cavity of aspect ratio $D = 10$ and $Ra = 70$ (for n odd, the dotted line represents the configuration n^- and the continuous line represents n^+).

Table 4: Transition angles of the multicellular configurations observed in $D = 10$ for $Ra = 70$ and $Ra = 100$ (the transition to odd number of cells is always to the positive branch n^+).

$D = 10$					
$Ra = 70$			$Ra = 100$		
n	Transition to	α_t	n	Transition to	α_t
1	7	30.6	1	7	32.4
7^+	1	34.4	7^+	1	45.0
7^-	9	3.2	7^-	15	4.1
8	9	8.5	8	9	6.4
9^+	1	31.4	9^+	1	40.0
9^-	7	13.3	9^-	13	8.8
10	9	11.0	10	9	15.5
11^+	7	26.4	11^+	7	33.7
11^-	9	9.8	11^-	9	14.4
12	7	7.2	12	11	11.7
13^+	11	19.9	13^+	9	25.9
13^-	11	5.8	13^-	11	10.6
14	13	3.6	14	13	8.4
15^+	13	11.6	15^+	11	20.9
15^-	13	2.3	15^-	12	7.4
—	—	—	16	15	5.6
—	—	—	17^+	13	15.2
—	—	—	17^-	15	4.5
—	—	—	18	17	3.0
—	—	—	19^+	15	9.2
—	—	—	19^-	17	2.0

and $n = 21$ were marginal though (lying in the range $0 \leq \alpha \leq 1°$) and were not included in Figure 10. For $Ra = 70$ it can be observed that $n = 9^+$ and $n = 11^+$ dominate the Nusselt number, but $n = 7^+$ prevails in a wider range of inclination angles, with a transition angle of $\alpha = 34.4°$.

In a similar way, for $Ra = 100$ (Figure 10), the highest Nusselt number is related to $n = 11^+$ and $n = 9^+$, whereas $n = 7^+$ is the most stable mode with a transition angle of $\alpha = 45°$. Figure 10 at $\alpha = 0$ shows that a large number of convective cells does not necessarily mean a high Nusselt number. It can be seen that from about 13 cells the Nusselt number of the n-odd cases starts decreasing. On the other hand, for even values of n, $n = 12$ provides the highest Nusselt number and from $n = 14$ it decreases. A common characteristic of Figures 9 and 10 is that there is a large decrease in the Nusselt number as the convective modes evolve towards single-cell. This is due to the large difference in the number of upwellings between multicellular and single-cell convection that large aspect ratios can accommodate.

5. Conclusion

A high resolution parametric study was carried out to provide a detailed view of the steady-state convective modes that exist in a 2D porous cavity heated from below as a function of the governing parameters of the system. The steady-state convection was grouped into two modes: multicellular convection and single cell convection. Multiple multicellular solutions were obtained for the horizontal cavity ($\alpha = 0$) based on the property of multiplicity. Each of these multicellular configurations was characterized by a given number of cells and by either of two possible distributions of the vorticity signs of the cells.

The configurations consisting of odd number of cells displayed two different behaviors regarding the Nusselt number as α was varied. On the one hand, when the predominant vorticity sign of the cells matched with the vorticity sign of the single-cell configuration for $\alpha \rightarrow 90°$, the Nusselt number increases up to a maximum. The Nusselt then decreases until the convective mode adopts either a different number of cells or the single-cell configuration. On the other hand, if the predominant vorticity signs are opposite to the single-cell natural convection, the Nusselt number decreases monotonically as α increases becoming unstable at comparatively smaller angles. In contrast, the solutions with even number of cells displayed a common behavior. Since in this case both distributions of vorticity signs contain the same number of clockwise and counterclockwise rotating cells, the Nusselt number of both forms behaved in the same way as a function of α. The Nusselt number decreased monotonically as α increased forming a zero-slope curve at $\alpha = 0$. These solutions also became unstable at small angles in comparison with the n-odd solutions.

Transition angles for all these solutions were also obtained. For a small aspect ratio ($D = 3$), the most stable convective modes (largest transition angles) also provided the highest Nusselt number. In contrast, the most stable modes in large aspect ratios did not necessarily mean a high heat transfer coefficient, a higher number of convective cells was necessary to enhance the convective heat transfer at the expense of a smaller transition angle. Furthermore, the results showed that multicellular convection can become unstable at larger angles than the critical angle predicted by Rees and Bassom [26] even when the aspect ratio is large. Some of the multicellular convective modes were destabilized and became single-cell at angles as large as $\alpha = 45°$. As a final remark, although 3D numerical modeling of this problem has shown considerably smaller transition angles to single cell convection [13], a high resolution parametric study in 3D has not been conducted yet. For this reason, alternative mathematical approaches such as continuation methods and also experimental work would be recommended in future work to understand the implications of these results in 3D systems.

Acknowledgement

This work was developed under the auspices of Consejo Nacional de Ciencia y Tecnología (CONACYT) and Cluff Geothermal Ltd. The first author is grateful to Dr. Andrew Rees of University of Bath for his insightful comments on this work. N. Karimi acknowledges the partial financial support by EPSRC through grant number EP/N020472/1 (Therma-pump).

References

[1] T. Graf, R. Therrien, Stable-unstable flow of geothermal fluids in fractured rock, Geofluids 9 (2009) 138–152.

[2] H. Gvirtzman, G. Garven, G. Gvirtzman, Thermal anomalies associated with forced and free ground-water convection in the dead sea rift valley, Geological Society of America Bulletin 109 (1997) 1167–1176.

[3] J. F. Wellmann, K. Regenauer-Lieb, How predictable are temperatures in geothermal resources, Proceedings of the World Geothermal Congress, Melbourne, Australia, 19-25 April 2015 (2015).

[4] A. C. Baytaş, I. Pop, Free convection in oblique enclosures filled with a porous medium, International Journal of Heat and Mass Transfer 42 (1999) 1047–1057.

[5] A. C. Baytaş, Entropy generation for natural convection in an inclined porous cavity, International Journal of Heat and Mass Transfer 43 (2000) 2089–2099.

[6] P. Meshram, S. Bhardwaj, A. Dalal, S. Pati, Effects of the inclination angle on natural convection heat transfer and entropy generation in a square porous enclosure, Numerical Heat Transfer Part A-Applications 70 (2016) 1271–1296.

[7] K. Khanafer, Fluid-structure interaction analysis of non-Darcian effects on natural convection in a porous enclosure, International Journal of Heat and Mass Transfer 58 (2013) 382–394.

[8] R. Bennacer, A. Tobbal, H. Beji, P. Vasseur, Double diffusive convection in a vertical enclosure filled with anisotropic porous media, International Journal of Thermal Sciences 40 (2001) 30–41.

[9] L. A. Tofaneli, M. J. S. de Lemos, Double-diffusive turbulent natural convection in a porous square cavity with opposing temperature and concentra-

tion gradients, International Communications in Heat and Mass Transfer 36 (2009) 991–995.

[10] P. H. S. Carvalho, M. J. S. de Lemos, Turbulent free convection in a porous square cavity using the thermal equilibirum model, International Communications in Heat and Mass Transfer 49 (2013) 10–16.

[11] M. J. S. de Lemos, Analysis of turbulent double-diffusive free convection in porous media using the two-energy equation model, International Communications in Heat and Mass Transfer 52 (2014) 132–139.

[12] P. H. S. Carvalho, M. J. S. de Lemos, Double-diffusive laminar free convection in a porous cavity simulated with the two-energy equation model, International Communications in Heat and Mass Transfer 82 (2017) 89–96.

[13] F. J. Guerrero-Martínez, P. L. Younger, N. Karimi, Three-dimensional numerical modeling of free convection in sloping porous enclosures, International Journal of Heat and Mass Transfer 98 (2016) 257–267.

[14] F. J. Guerrero-Martinez, P. L. Younger, N. Karimi, S. Kyriakis, Three-dimensional numerical simulations of free convection in a layered porous enclosure, International Journal of Heat and Mass Transfer 106 (2017) 1005–1013.

[15] D. A. Nield, A. Bejan, Convection in Porous Media, 4th ed., Springer, New York, 2013.

[16] C. W. Horton, F. T. Rogers, Convection currents in a porous medium, Journal of Applied Physics 16 (1945) 367–370.

[17] E. Lapwood, Convection of a fluid in a porous medium, Proceedings of the Cambridge Philosophical Society 44 (1948) 508–521.

[18] J. Elder, Steady free convection in a porous medium heated from below, Journal of Fluid Mechanics 27 (1967) 29–48.

[19] J. M. Straus, Large-amplitude convection in porous-media, Journal of Fluid Mechanics 64 (1974) 51–63.

[20] M. D. De La Torre Juárez, F. H. Busse, Stability of 2-dimensional convection in a fluid-saturated porous-medium, Journal of Fluid Mechanics 292 (1995) 305–323.

[21] T. Kaneko, M. F. Mohtadi, K. Aziz, Experimental study of natural convection in inclined porous media, International Journal of Heat and Mass Transfer 17 (1974) 485–496.

[22] S. L. Moya, E. Ramos, M. Sen, Numerical study of natural-convection in a tilted rectangular porous material, International Journal of Heat and Mass Transfer 30 (1987) 741–756.

[23] S. A. Bories, M. A. Combarnous, Natural-convection in a sloping porous layer, Journal of Fluid Mechanics 57 (1973) 63–79.

[24] M. Sen, P. Vasseur, L. Robillard, Multiple steady-states for unicellular natural-convection in an inclined porous layer, International Journal of Heat and Mass Transfer 30 (1987) 2097–2113.

[25] D. S. Riley, K. H. Winters, A numerical bifurcation study of natural-convection in a tilted two-dimensional porous cavity, Journal of Fluid Mechanics 215 (1990) 309–329.

[26] D. A. S. Rees, A. P. Bassom, The onset of Darcy-Bénard convection in an inclined layer heated from below, Acta Mechanica 144 (2000) 103–118.

[27] E. Báez, A. Nicolás, 2D natural convection flows in tilted cavities: Porous media and homogeneous fluids, International Journal of Heat and Mass Transfer 49 (2006) 4773–4785.

[28] D. Evans, J. Raffensperger, On the stream function for variable-density groundwater flow, Water Resources Research 28 (1992) 2141–2145.